Desalination and Water Treatment
www.deswater.com

doi: 10.1080/19443994.2015.1042056

57 (2016) 11048–11065
May

Taylor & Francis
Taylor & Francis Group

A poly(sulfobetaine) hollow fiber ultrafiltration membrane for the treatment of oily wastewater

Qian Li, Zhi-Qin Yan, Xiao-Lin Wang*

Beijing Key Laboratory of Membrane Materials and Engineering, Department of Chemical Engineering, Tsinghua University, Beijing 100084, P.R. China, Tel. +86 010 62794741; emails: qian-li@mail.tsinghua.edu.cn (Q. Li), yanzqin@126.com (Z-Q. Yan), xl-wang@tsinghua.edu.cn (X-L. Wang)

Received 10 June 2014; Accepted 10 April 2015

ABSTRACT

A poly(sulfobetaine) (PSB) hollow fiber ultrafiltration (UF) membrane with permanent hydrophilicity was obtained by forming a thick PSB layer on the surface and subsurface of poly(vinylidene fluoride) (PVDF) hollow fiber microfiltration (MF) membrane. After immersed in 40 mmol/L NaCl solution, the sieving layer (PSB layer) of the UF membrane stretched completely. The PSB hollow fiber UF membrane with sieving layer and MWCO of 5.2 μm and 85–105 kDa, respectively, was formed, which contributed to the great improvement of hydrophilicity, membrane strength, and thermal property. The PSB hollow fiber UF membrane showed a good filtration performance with the permeate flux and oil rejection of ≈300 L/m^2h and >80% at 0.1 MPa, respectively, and an excellent anti-oil-fouling property with the relative flux recovery of >98% during the filtration of the oily water with 40 mmol/L NaCl and at pH 6. More than 90% of oil droplets were rejected by the membrane while the soluble oil permeated through the membrane. The fouling mechanisms involved in the MF and UF processes of the oily water were analyzed using Hermia's models. The results showed that intermediate blocking and cake layer formation or combinations of them were found during the UF experiments for the PSB hollow fiber membrane. By means of the simple immersion, the transformation of surface pores between "opened" and "closed" during the filtration of the oily water can be obtained. The results extended the application of PSB hollow fiber membrane in treatment of oily wastewater and purification of water.

Keywords: Treatment of oily wastewater; PSB hollow fiber UF membrane; Anti-oil-fouling performance; Smart behavior; Fouling mechanism

1. Introduction

Oily wastewater is one of the main pollutants emitted into water by industry and domestic sewage [1–3]. The industries such as petrochemical processing, petroleum refining, and oil and natural gas production generate large volumes of oily wastewaters [2–4]. Lots of physical, chemical, and biological techniques are usually used to treat these wastes before they are disposed in the environment or reused as agricultural water [1–4]. However, these treatments of produced water are often expensive, and in constant need of improvement as discharge specifications tighten [5,6]. Ultrafiltration (UF) is very promising to treat the

---

*Corresponding author.

wastewater [3]. UF membrane can remove essentially all free and dispersed oil from wastewater, and the permeate is consistently able to meet Oil and Gas Standards for discharge [2–6]. The polymers such as poly(vinylidene fluoride) (PVDF) and poly(ether sulfones) (PES)/polysulfone (PSF) have been recognized as the most attractive polymers in membrane industry due to their extraordinary mechanical property, high chemical resistance, and good thermal stability [7–9]. But these membranes have been limited in the treatment unit of oily wastewater by economic obstacles because of the severe membrane fouling [8]. On the other hand, for a typical UF membrane, the pore size is fixed after preparation and the membrane exhibits an uncontrollable sieving/selectivity, which limits its application scope [10]. Therefore, it is increasingly desirable to prepare a UF membrane with the anti-oil-fouling performance and the capability to adjust the sieving/selectivity, i.e. the controllable "open"/"close" behavior.

In our preceding work, a novel hollow fiber UF membrane with excellent anti-fouling performance has been prepared by cross-linking reaction with poly (vinyl pyrrolidone) (PVP) and subsequent graft polymerization of a sulfobetaine (SB) monomer, 3-(methacryloylamino) propyl-dimethyl–(3-sulfopropyl) ammonium hydroxide (MPDSAH) from the PVDF membrane [7]. SB and its polymer poly(sulfobetaine) (PSB) have been used to functionalize various porous membranes due to the strong hydration and environment sensitivities [11–28]. The unique properties of PSB could be attributed to its zwitterionic structure, which bears both negative (sulfonate, $–SO_3^-$) and positive (amide, $–^+NH–$) charge units on each monomer, but the functionality of PSB layer to control membrane property is influenced by its density on/in the membrane. Due to the electrostatic interaction and hydrogen bond, the PSB on the membrane surface often displays a strong hydration causing a repulsive force to the particle/oil droplet at specific separation distances [8,12,15,16]. If the PSB chains are long enough, the electrostatic energy between the opposite charges of PSB is larger than the energy required for dehydration, thus polymer chains will associate through intra- and/or inter-chain interactions and form a super-collapsed state [26]. The presence of inorganic electrolyte can shield the associations of PSB chains and lead to a swelling and stretching structure in the aqueous solution, which is called "anti-polyelectrolyte effect" [27,28]. Therefore, the stretching of PSB layer which formed on the membrane surface would make the surface pores "closed," while the collapsed structure of PSB chains would "open" the surface pores of membrane. A polyMPDSAH layer was formed on and in the membrane, and the selective separation for proteins through the membrane was confirmed in our preceding work. However, for UF membrane with high sieving capability, a sufficient thickness of PSB layer should be grafted on the PVDF support membrane. In addition, compared to the protein solution, the oily wastewater is involved more commonly in the field of wastewater treatment. Therefore, the oil separation from oily solution through such hollow fiber UF membrane is necessary to be investigated.

In this work, a PSB hollow fiber UF membrane was prepared by forming a thick polyMPDSAH layer on the PVDF support membrane. The effect of NaCl concentration on the morphology and properties of the PSB hollow fiber UF membrane was discussed in detail to obtain the complete stretching state of polyMPDSAH. The filtration performances of oily water through the membranes were studied under different conditions. Four kinds of fouling models were used to analyze the fouling mechanisms involved in the UF processes of oily water.

2. Experimental

2.1. Materials and reagents

Poly(vinylidene fluoride) (PVDF) hollow fiber microfiltration (MF) membrane with average pore diameter of 0.15 μm and porosity of 70% was prepared via thermally induced phase separation (TIPS) method. The PVDF hollow fiber membrane with internal and external diameter of 0.8 and 1.3 mm was sliced into cylindrical strips with length of 20–30 cm. Poly(vinyl pyrrolidone) (PVP K30, $M_w = 35{,}000$) was purchased from BoaiNky Pharmaceuticals Ltd. (Henan, China). The PVP was dried in vacuum at 60 ± 1℃ for 8 h before used. Ascorbic acid (AscA), N,N,N′,N′,N′-pentamethyldiethylenediamine (PMDETA), copper chloride ($CuCl_2$), N,N′-methylene bisacrylamide (MBAA), and 3-(methacryloylamino) propyl-dimethyl - (3-sulfopropyl) ammonium hydroxide (MPDSAH) were obtained by Beijing Hengye Zhongyuan Chemical Co., Ltd (Beijing, China). Tween 80, sodium hypochlorite (NaClO), ceric ammonium nitrate (CAN), 2-hydroxyethyl methacrylate (HEMA), potassium persulfate ($K_2S_2O_8$), sodium hydroxide (NaOH), chlorhydric acid (HCl), nitric acid (HNO_3), sodium chloride (NaCl), dextran (M_w = 20,000, 40,000, 100,000, respectively), and polyethylene oxide (PEO; M_w = 200,000, 300,000, respectively) were purchased from Sinopharm Chemical Reagent Beijing Co., Ltd (China). Super vacuum pump oil (GS-1) was brought by from Beijing Hua Te Lubricant Oil Co., Ltd (China).

2.2. Preparation of the UF membrane

An environment sensitive membrane with a thick polyMPDSAH layer was firstly prepared by the cross-linking reaction of PVP and subsequent grafting polymerization of MPDSAH on and in the PVDF hollow fiber MF membranes, then, a PSB hollow fiber UF membrane was obtained after the swelling process in electrolyte solution, which is similar to our preceding work [7].

Firstly, the PVDF membrane (M0) was soaked in the aqueous solution containing cross-linking agent $K_2S_2O_8$ (0.4 wt%) and polymer PVP K30 (5 wt%) at 90 ± 1℃ for 6 h. The cross-linked membrane (PVDF-cl-PVP, MCP) was washed by deionized water for 24 h and then dried under vacuum.

Secondly, the dried M0 or MCP was placed in a dry flask containing HEMA, $CuCl_2$, PMDETA, pure water, and reacted under nitrogen protection at 40℃ for 30 min. A degassed solution of AscA was transferred into the flask under nitrogen protection and polymerized for 6 h. After washed and dried, the membrane was placed into a dry flask and mixed with 200 mL of degassed solution containing CAN, HNO_3, MPDSAH, and MBAA under nitrogen protection at 40℃. After 3 h, the grafted membrane (polyMPDSAH-g-PVDF, MM, grafting amount = 682 $\mu g/cm^2$ or polyMPDSAH-g-PVDF-cl-PVP, MMCP, grafting amount = 721 $\mu g/cm^2$) was thoroughly washed with 0.05 mol/L of phosphate-buffered saline (PBS, pH 7.4) and pure water for 1 h, respectively.

Thirdly, the prepared MMCP was soaked in a closed vessel containing NaCl (0, 10, 20, 30, 40, 50, and 60 mmol/L) aqueous solution at 60 ± 1℃. The membrane was stored in the electrolyte solution until the membrane was removed and washed by pure water for 10 times, and then dried under vacuum to make samples for membrane characterization.

The code name and preparation conditions of various membranes are listed in Table 1.

2.3. Membrane characterization

The surface chemical compositions of the membranes were characterized using attenuated total reflectance (ATR)-Fourier transform infrared (FTIR) spectroscopy (Nicolet 6700, ThermoFisher Scientific, USA) and X-ray photoelectron spectroscopy (XPS) (ULVAC-PHI, Japan). During the ATR-FTIR measurements, zinc selenide (ZnSe) was applied as an internal reflection element and each spectrum was captured by 64 averaged scans at the resolution of 4 cm^{-1}. XPS measurement was performed using an Al–Mg anode target and the X-ray source was run at 250 W with an electron take off angle of 45^o relative to the sample surface. The base pressure of the analyzer chamber was about 5×10^{-7} Pa. The chemical compositions of membrane cross section were measured by the mapping technique of ATR-FTIR spectroscopy under the preservation of liquid nitrogen. The ATR-FTIR mapping from the outside surface in cross section was graphed out for each membrane sample.

The outside surface and outer cross section morphologies of the membrane were observed using a scanning electron microscope (SEM) (JSM7401, JEOL, Japan) under standard high vacuum conditions at magnification of 10,000× and 5,000×, respectively. The surface mean pore size (SMP, μm) was analyzed using the software Image-Pro Plus 6.0.

Tensile strength (MPa) and elongation ratio (%) of the membranes were measured by material test machine (AGS-J20N, Shimadzu, Japan) at a loading velocity of 30 mm/min.

Static and dynamic contact angles between water and dry membrane sample were measured by a

Table 1
Preparation conditions and XPS surface compositions of various membranes

Code	Membrane	NaCl concentration (mmol/L)	Content (mol%) F	C	O	N	S
M0	PVDF	–	33	67	0	0	0
MCP	PVDF-cl-PVP	–	14	61	20	5	0
MMCP	polyMPDSAH-g-PVDF-cl-PVP	–	7	54	15	17	7
MMCP-10	polyMPDSAH-g-PVDF-cl-PVP	10	6	54	16	17	7
MMCP-20	polyMPDSAH-g-PVDF-cl-PVP	20	6	55	16	16	7
MMCP-30	polyMPDSAH-g-PVDF-cl-PVP	30	7	53	15	17	8
MMCP-40	polyMPDSAH-g-PVDF-cl-PVP	40	6	56	15	16	7
MMCP-50	polyMPDSAH-g-PVDF-cl-PVP	50	6	54	16	16	8
MMCP-60	polyMPDSAH-g-PVDF-cl-PVP	60	6	57	15	15	7

contact angle meter (OCA 20, DataPhysics Instruments GmbH, Germany) at 25℃. Water (1 μL) was carefully dropped on the dry sample with an automatic piston syringe. The contact angle value of each sample was measured at three various positions of one sample. In order to avoid the damage of pore structure due to drying, the free water fraction (FWF) of swelled membrane was estimated by the differential scanning calorimetry (DSC) measurement (Q 2000, TA Instruments, US) [7].

The thermal properties of the dried membranes were determined by DSC and Thermal Gravimetric Analysis (TGA) (STA 409PC Luxx, NETZSCH, Germany), in a dry nitrogen atmosphere. The sample of DSC was heated from 50 to 200℃ with a heating rate of 10℃/min, and the sample of TGA was heated from 50 to 900℃ with a heating rate of 10℃/min.

2.4. Rejection experiment

Though most commercial applications involve cross-flow modules, dead-end filtration studies are valuable as a “worst case scenario” for fouling [2]. Therefore, a self-made dead end filtration was used in this work to characterize the rejection and permeate performance of the wet membranes. The setup was used for rejection experiments with dextrans ($M_w = 20{,}000$, 40,000, 100,000, respectively) and PEOs ($M_w = 200{,}000$, 300,000, respectively) at the concentration of 0.50 g/L. The feed solutions were placed in an ultrasonic machine (KQ-100 DB, Kun Shan Ultrasonic Instruments, China) at 40% of output power in order to minimize the concentration polarization effects. The concentration of samples from the feed and collected permeate were analyzed by Total Organic Carbon (TOC) (TOC-V$_{cpn}$ Instrument, Shimadzu, Japan). The rejection for dextran or PEG was calculated using Eq. (1). M_W which was rejected to 90% is defined as the molecular weight cut-off (MWCO) of the membrane [29]. The hydrodynamic diameter values (nm) of dextran and PEO were calculated from M_W using Eq. (2) [29] for dextran and Eq. (3) [30] for PEO, which were used to express the approximate apparent pore diameter values (D, nm) of membranes.

$$R_i = \left(1 - \frac{C_P}{C_F}\right) \times 100 \tag{1}$$

$$D(\text{dextran}) = 0.096\text{M}_W{}^{0.59} + 0.128\text{M}_W{}^{0.5} \tag{2}$$

$$D(\text{PEO}) = 2.088 \times 10^{-3}\text{M}_W{}^{0.587} \tag{3}$$

where C_P and C_F are the dextrans or PEOs in the feed and permeate solutions, respectively.

2.5. Cyclic filtration tests

In this section, the membrane was stored in the electrolyte solution. Before tests, the membrane was washed by pure water for more than 10 times to remove the electrolyte, the covering the membrane surface. Then, the same setup described in *Section 2.4* was applied to characterize the permeate performance of the wet membranes in the oily water at the pressure of 0.05–0.20 MPa. Oil filtration experiments were performed on the 1 L oily water feed consisted of 1,500 ppm GS-1/Tween 80 (9:1), which had been emulsified by blending for 12 h at 50 W in an ultrasonic machine. The droplet size of the oil sample with different NaCl or pH were measured by a laser diffraction particle size analyzer (Mastersizer 3,000, Malvern Instruments, UK) with refracting index of 1.52 and absorptivity of 0.00001, which are listed in Table 2. The effects of NaCl concentrations and pH environments on the permeate flux of the oily water through various membranes were investigated.

Firstly, the averaged pure water flux (L/m^2 h) was determined by successively sampling every 10 min in 30 min. After the filtration step of pure water, the filtration step of the oily water containing NaCl (0, 20, 40 mmol/L) was performed and repeated in different pH environments (pH 4, pH 6, and pH 8). The pH of feed solution was adjusted by NaOH or HCl solution. The volume of permeate was collected every 10 min and then measured using a balance. The flux of the membrane ($J_{v,i}$, L/m^2 h) was calculated according to Eq. (4):

$$J_{v,i} = \frac{V_i}{A \cdot \Delta t} \quad (i = 1, 2, 3) \tag{4}$$

where V_i, A, and Δt are the permeate volume (L), outside surface area of the membrane (m^2), and permeation time (h), respectively.

Table 2
Droplet size (D_v 10) of oil-in-water emulsions with different NaCl or pH

	Droplet size (μm)		
NaCl concentration (mmol)	pH 4	pH 6	pH 8
0	–	2.53	2.48
20	–	2.92	3.23
40	–	1.84	2.37

Then, the used membrane was successively washed by 0.5 g/L sodium hypochlorite (NaClO) solution (25 ± 1˚C) and NaCl aqueous solution (60 ± 1˚C) for 30 min, respectively. After rinsing the membrane, the fluxes (L/m^2 h) of pure water and oily water were measured again. Then, the three cyclic filtrations were performed.

To evaluate the fouling resistance of membrane, the relative flux recovery (RFR_i, %) was calculated:

$$\mathrm{RFR}_i\ (\%) = \frac{J_{\mathrm{v}_{\mathrm{H_2O}},i}}{J_{\mathrm{v}_{\mathrm{H_2O}},0}} \times 100\ (i = 1, 2, 3) \tag{5}$$

where $J_{\mathrm{v}_{\mathrm{H_2O}},i}$ is the pure water flux during ith cycle filtration (L/m^2 h).

The concentrations of oil in the feed and permeate solutions were measured immediately after collection using an ultraviolet–visible spectrophotometer (TU-1810, Purkinje General, China) at 531 nm. The rejection (R_i, %) was calculated by Eq. (1).

Table 3
Model equations for various fouling mechanisms

Fouling mechanism	Model equation
Complete pore blocking	$\mathrm{Ln}(J) = \mathrm{Ln}(J_0) + K_{\mathrm{co}}t$
Standard pore blocking	$1/J^{1/2} = 1/{J_0}^{1/2} + K_{\mathrm{s}}t$
Intermediate pore blocking	$1/J = 1/J_0 + K_iAt$
Cake layer formation	$1/J^2 = 1/{J_0}^2 + K_{\mathrm{cl}}t$

2.6. Theoretical background

Focused on the 1st cycle of filtration, Hermia's models were used to interpret the fouling phenomenon occurring in the MF and UF of oily water, including cake layer formation, intermediate pore blocking, standard pore blocking, and complete pore blocking [28,31]. The four model equations are given in Table 3. The calculated model constants (K) and R^2 values were obtained by using OriginPro 8.6.

3. Results and discussion

3.1. Formation and characterization of the PSB UF membrane

In our preceding study, we have reported that a UF membrane based on the PVDF hollow fiber MF membrane can be designed by an environment sensitive membrane with a dense polyMPDSAH layer on the surface and subsurface of membrane which was firstly prepared via the cross-linking reaction with PVP and subsequent grafting polymerization of MPDSAH. Then, the chains of polyMPDSAH layer were expanded and the UF membrane was obtained by the swelling process in electrolyte solutions. We

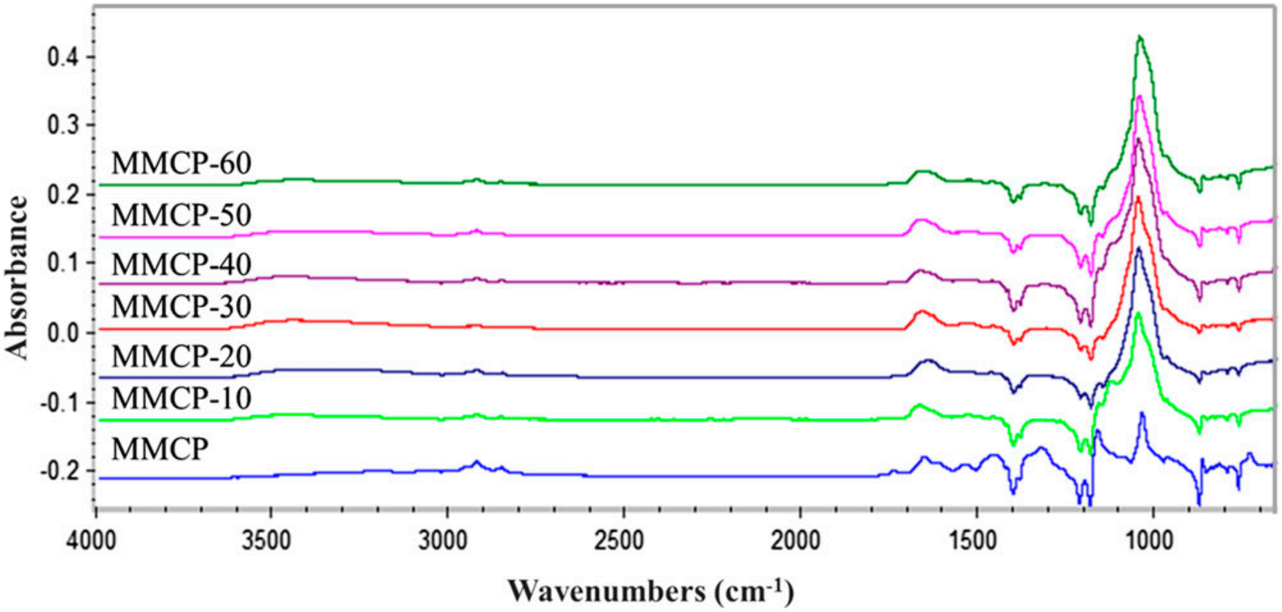

Fig. 1. ATR-FTIR difference spectra of the outside surfaces of MMCP, MMCP-10, MMCP-20, MMCP-30, MMCP-40, MMCP-50, and MMCP-60.

have found that the shielding effect of 1–1 type electrolyte solution (NaCl) on the intra- and/or inter-chain associations of polyMPDSAH chains was superior to others [7]. Therefore, in this study, the effect of NaCl concentration on the characterization of the polyMPDSAH hollow fiber UF membrane will be investigated in detail.

The code of various membranes can be found in Table 1. The difference spectrum between each membrane and M0 is shown in Fig. 1. For the spectra of MMCP, additional adsorption at 1,650 cm^{-1}, which was attributed to the vibration of –C=O in PVP was observed due to the cross-linking reaction between PVP and PVDF. The ATR-FTIR spectra of MMCP, MMCP-10–MMCP-60 exhibited peak at 1,037 cm^{-1} which was due to the vibration of sulfonate ($–SO_3^-$) group existing in the structure of MPDSAH. With the increase of NaCl concentration, the intensities of characteristic peaks increased obviously, meaning that the increase in electrolyte concentration was favorable to form the more extended conformation of polyMPDSAH. Table 1 lists the relative element contents measured by XPS analysis for various membranes. The relative content of sulfur which was an indicative atom for MPDSAH increases from 0 mol% for M0, and MCP to more than 5 mol% for MMCP. Besides, the amount of polyMPDSAH on the MMCP-10–MMCP-60 surface was equal to that on the MMCP surface, indicating that the loss or hydrolysis of the grafted MPDSAH polymer layer on the membrane was negligible during the swelling process in the electrolyte solution.

Fig. 2 illustrates the ATR-FTIR mapping curves through the cross section from the outside surface of M0, MMCP, and MMCP-40. The adsorption peaks at 1,037 and 1,650 cm^{-1} were found in the spectra of the outer cross section of MMCP and MMCP-40. The peaks could be attributed to the vibration of –NH–,

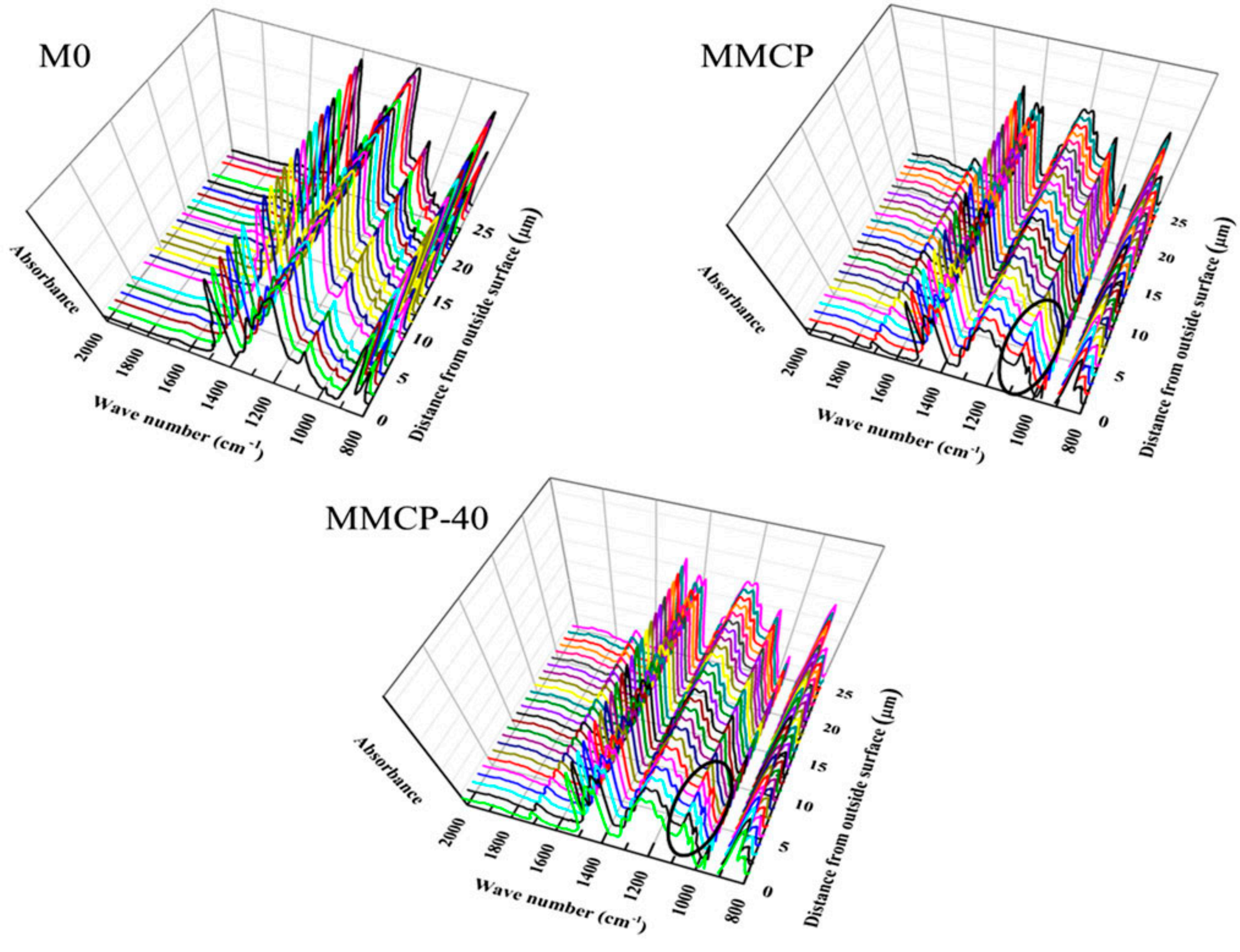

Fig. 2. ATR-FTIR Mapping of the cross section of M0, MMCP, and MMCP-40.

and $–SO_3^-$ in PVP and polyMPDSAH chains, which meant that the MPDSAH monomers had entered the membrane bulks and grafted from the surface of inner pores except to the membrane surfaces. Moreover, for MMCP, the characteristic peaks appeared in the mapping spectrum at 1 μm from the outside surface, while for MMCP-40, the characteristic peaks were observed in the mapping spectrum at 5 μm from the outside surface, indicating that the polyMPDSAH layer of MMCP-40 was nearly five times thicker than that of MMCP.

The surface and cross section morphologies of various membranes were examined by SEM, as shown in Fig. 3. Compared with the nascent PVDF membrane (M0), the opening of the partial pores at the surface of MMCP appeared to be significantly reduced because the zwitterionic polymer chains covered them after cross-linking reaction and grafting polymerization. It could be observed that the pores on the surface of MMCP-40 and MMCP-60 were fully covered due to the complete swelling of polyMPDSAH chains on the surface and subsurface of the membrane.

The surface pore diameter could be characterized by SEM combined with image analysis software. The surface mean pore size (SMP) and pore size distribution of various membrane samples are shown in

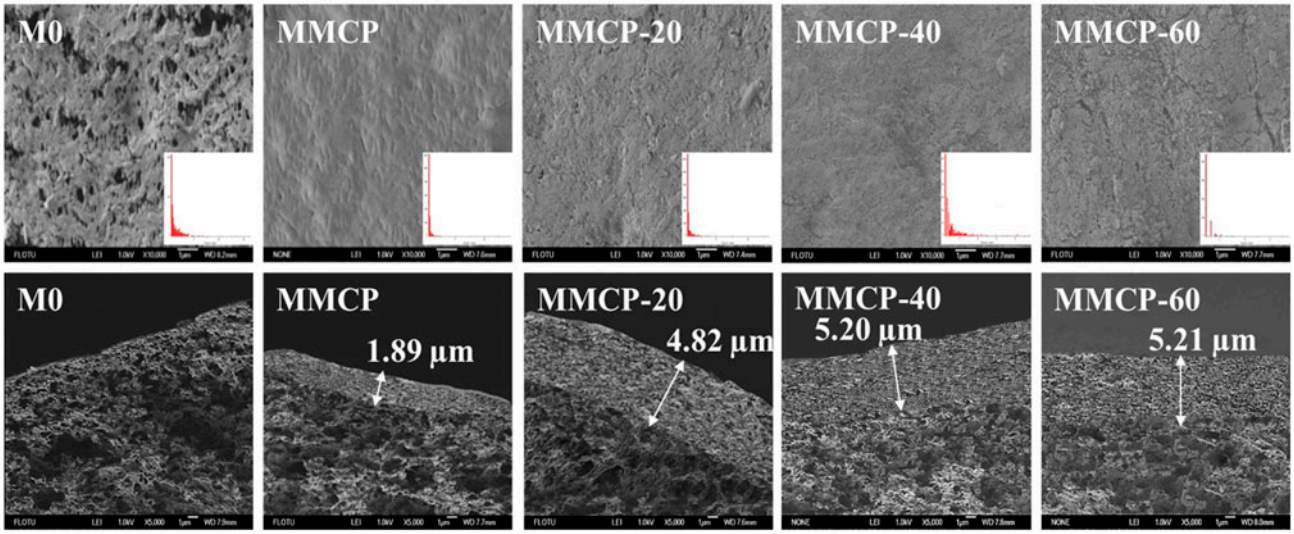

Fig. 3. SEM images of the outside surfaces (upside) and the outer cross sections (downside) of M0, MMCP, MMCP-20, MMCP-40, and MMCP-60.

Table 4
Structure, strength, hydrophilicity, and rejection properties of various membranes

		Membrane strength		Hydrophilicity			
Code	SMP (μm)	Tensile strength (MPa)	Elongation ratio (%)	Contact angle (°)	FWF at pH 7	MWCO (kDa)	$D_{\text{cut-off}}$ (μm)
M0	0.109	4.1	95.9	83.3 ± 2.1	0.08	–	–
MMCP	0.051	3.9	92.5	78.6 ± 1.8	0.49	–	–
MMCP-10	0.035	4.3	96.9	45.4 ± 1.9	0.51	290–310 (PEO)	0.034
MMCP-20	0.010	4.2	97.1	39.3 ± 2.0	0.58	95–115 (Dextran)	0.012
MMCP-30	0.010	4.3	98.0	30.2 ± 2.1	0.62	90–110 (Dextran)	0.012
MMCP-40	0.010	4.3	100.1	25.6 ± 1.8	0.69	85–105 (Dextran)	0.012
MMCP-50	0.010	4.4	99.9	25.5 ± 1.7	0.70	85–105 (Dextran)	0.011
MMCP-60	0.009	4.3	100.1	28.7 ± 1.9	0.68	85–105 (Dextran)	0.011

Table 4 and Fig. 3. With the increasing of NaCl concentration, the distribution of surface pore size of the swelled polyMPDSAH-g-PVDF-cl-PVP membranes became uniform and the SMP was much smaller. The swelled polyMPDSAH layer of the membrane can be seen from the SEM images of outer cross section of membranes in Fig. 4. The swelling layer thickness followed the trend of MMCP-60 (5.21 μm) ≈ MMCP-40 (5.20 μm) > MMCP-20 (4.82 μm) > MMCP (1.89 μm), which was opposite to the result of SMP. It confirmed that the swelling layer of the membrane varied from 0 to >5 μm by altering the immersion conditions. In addition, when the NaCl concentration was increased to 40 mmol/L, the thickness of polyMPDSAH layer was not enhanced obviously with the further addition of NaCl into the swelling solution. It meant that the polyMPDSAH layer on the surface and subsurface of membrane swelled and stretched completely at the NaCl concentration of 40 mmol/L.

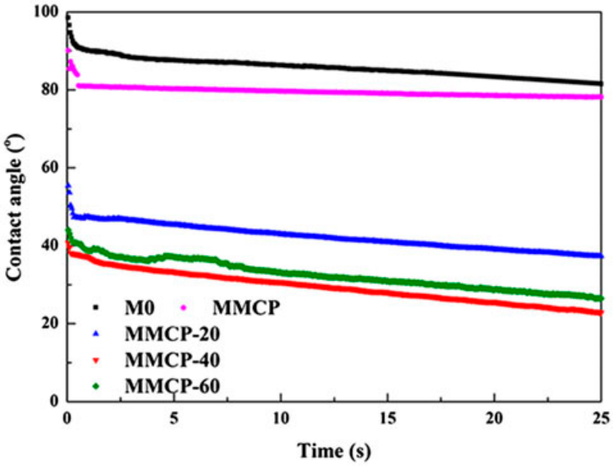

Fig. 4. Dynamic contact angles of the outside surfaces of M0, MMCP, MMCP-20, MMCP-40, and MMCP-60.

The tensile strength and elongation ratio of various membranes were measured to represent the membrane mechanical properties, which are shown in Table 4. With the increase of the NaCl concentration, the tensile strength and elongation ratio of membranes increased due to the increase in the thickness of swelled polyMPDSAH layer. The hydrophilicity is an important membrane property which affects the membrane permeability. The static and dynamic contact angles were measured to confirm the hydrophilization effect of the dry membrane and the FWF of swelled membrane was estimated by DSC method to show the hydrophilic property of the wet membrane, as shown in Fig. 4 and Table 4. The water droplet penetrated into membrane bulk gradually and the contact angle on the outside surface decreased with time. The velocity of water droplet penetrating into membrane was faster on the more hydrophilic membrane surface. As demonstrated in Fig. 4, the descent speed of water contact angles on the membrane surfaces followed the trend of M0 < MMCP < MMCP-20 < MMCP-40 ≈ MMCP-60, which was contrary to the values of the static contact angles. The values of FWF in Table 4 changed in the same order with the descent speed of dynamic contact angles: M0 (0.08) < MMCP (0.49) < MMCP-20 (0.58) < MMCP-40 (0.68) ≈ MMCP-60 (0.69). Combined with the results from Fig. 3, it was deduced that the thicker swelling layer of polyMPDSAH contributed to the higher hydrophilicity.

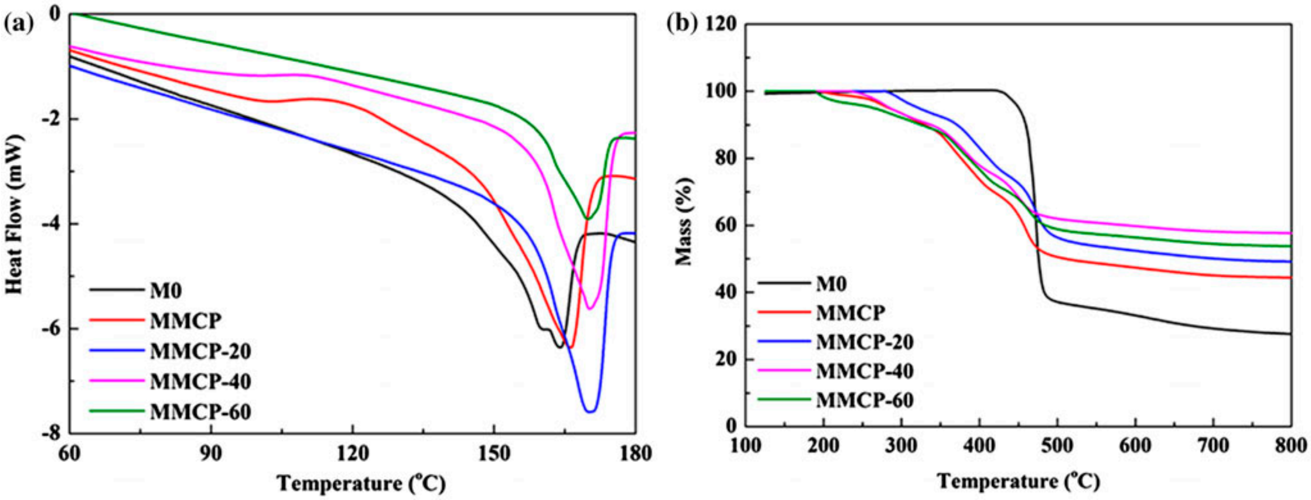

Fig. 5. Thermal properties of M0, MMCP, MMCP-20, MMCP-40, MMCP-60 (a) DSC curves and (b) TGA curves.

The thermal properties of various membranes can be found in Fig. 5. The DSC curves in Fig. 5(a) shows that the melting temperature increased after the grafting polymerization of MPDSAH from the PVDF membrane due to the higher melting point of MPDSAH (190˚C) than that of PVDF (170˚C) [9,31]. The swelling of polyMPDSAH on the surface and subsurface of membrane contributed to the further increase of melting temperature. It meant that the thermal property of swelled polyMPDSAH-g-PVDF-cl-PVP membrane was improved slightly. The mass loss of various membranes with the temperature is shown in Fig. 5(b). Compared to M0, the initial temperature of mass loss was lower for MMCP and MMCP-20–MMCP-60 due to the swelling layer of polyMPDSAH. However, when the temperature was as high as 800˚C, the reduction of membrane mass for MMCP and MMCP-20–MMCP-60 was much less than that for M0.

In the preceding study, we have confirmed that a controllable selectivity of the environment sensitive membrane can be obtained by altering the structure of the sieving layer (i.e. polyMPDSAH layer). To estimate the membrane selectivity, the rejection curves were built by plotting the rejection values vs molecular weight (M_W), as shown in Fig. 6. MMCP showed a gentle curve and the values of tested rejection were lower than 80% due to the relatively large pore size and the collapsed structure of polyMPDSAH layers (see insert images in Fig. 6). It was interesting that the swelling of polyMPDSAH layer on and in the membrane enhanced the membrane rejection enormously. For MMCP-20–MCP-60, the rejection curves show the fast increase in the rejection with M_W until to 90%. The collected data from the rejection experiments are summarized in Table 4. It appeared that pore diameters ($D_{\text{cut-off}}$) calculated from dextran or PEO data matched the analyzed SMP and the sieving layer thickness (Fig. 3). An increase in NaCl concentration reduced the membrane MWCO as a result of the thickening of the swelling layer on the outside surface and subsurface. In short, MMCP-40 showed a good hydrophilicity and an excellent UF performance due to the complete swelling of polyMPDSAH layer.

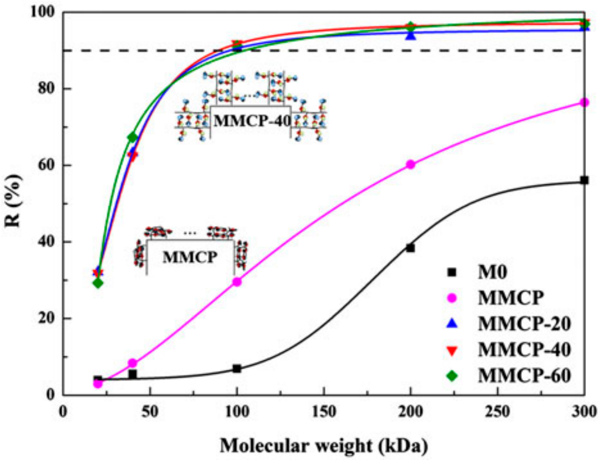

Fig. 6. Rejection curves of M0, MMCP, MMCP-20, MMCP-40, and MMCP-60.

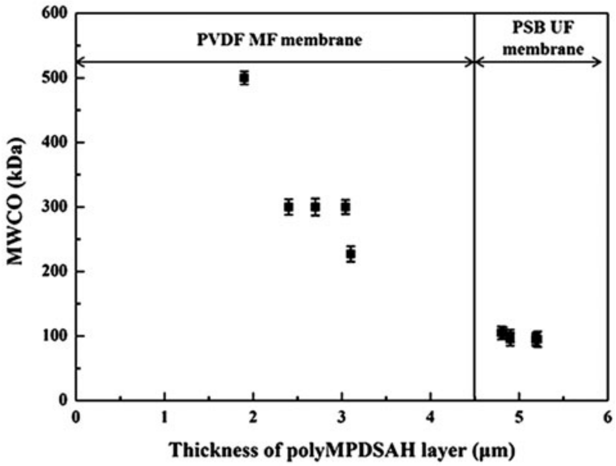

Fig. 7. Relationship between the thickness of polyMPDSAH layer and the MWCO [7].

Combing the previous experimental results and the data obtained in this work, the relationship between the thickness of polyMPDSAH layer and the MWCO can be found in Fig. 7 [7]. In conclusion, the sufficient thickness of polyMPDSAH layer played an important role in the sieving capability of the UF membrane. It meant that the PSB hollow fiber UF membrane formed as the thickness of polyMPDSAH layer more than 4.5 μm.

3.2. *Filtration performance of oily water through the PSB UF membrane*

For the application of wastewater treatment, the membrane fouling of UF membrane due to the oil droplets is one of the major problems. Thus, it is of great significance to improve the anti-oil-fouling property of membrane and enhance the oil rejection (i.e. separation efficiency). In this section, the filtration performance of the oily water through M0, MMCP, and MMCP-40 will be investigated. The effects of pH and NaCl concentration in the oily water on the performance of membrane will be discussed in detail. M0 and MMCP were used as the MF membrane for oil separation, while the MMCP-40 was used as the PSB UF membrane for oil separation due to its optimum

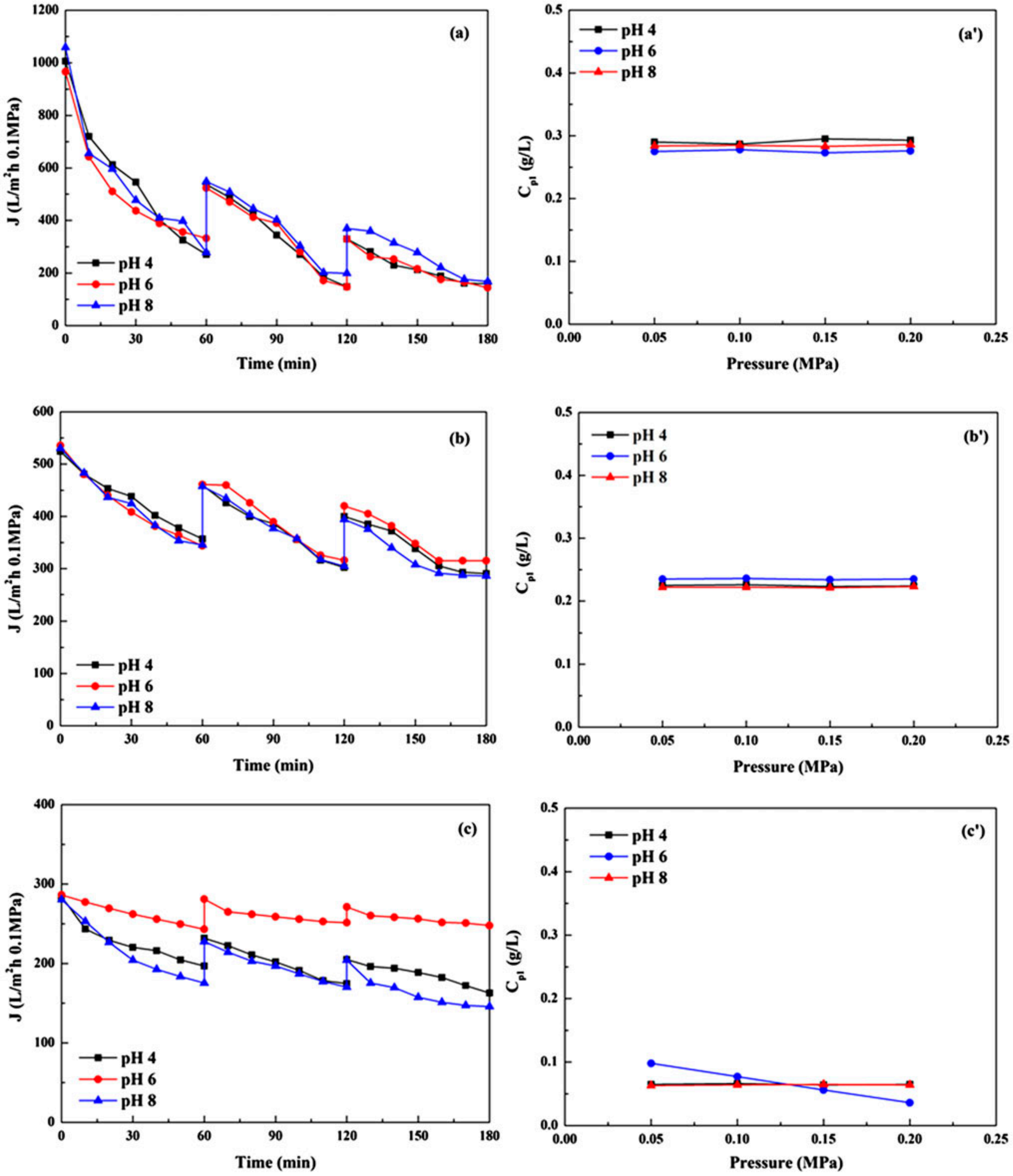

Fig. 8. Filtration decline behavior and permeate concentration after 1st cycle filtration of (a-a´) M0, (b-b´) MMCP, and (c-c´) MMCP-40 in the oil-in-water emulsion with different pH (at NaCl concentration of 40 mmol/L).

properties and performances among the tested UF membranes.

Fig. 8(a)–(c) presents the flux versus time for the oil filtration experiments performed using M0, MMCP, and MMCP-40 in the different pH environment. For each membrane, the permeate flux declined rapidly at the start of filtration and the relatively steady permeation flux was finally observed at the later stage of each filtration circle, suggesting that the adsorption/deposition and the back diffusion of the oil droplets reached an equilibration at the membrane surface. For M0, the flux in the second and third cycles of the oily water filtration was much lower than that in the first cycle. For MMCP and MMCP-40, the initial fluxes decreased due to the coverage of polyMPDSAH layer on the surface and subsurface of membrane. But strong hydration and hydrophilicity of polyMPDSAH contributed to the reduction of filtration decline behavior, as shown in Fig. 8(b) and (c). Especially for MMCP-40, the flux was nearly constant through the whole filtration circle, manifesting the very little membrane fouling as a result of the completely stretched polyMPDSAH chain.

The pH of oily water had little impact on the filtration performance of M0 and MMCP, as illustrated by Fig. 8(a) and (b), respectively. It could be attributed to the inert property of PVDF support membrane for M0, and the collapsed structure of thin polyMPDSAH layer for MMCP. On the contrary, MMCP-40 showed an obvious difference in the filtration performance of oily solution with different pH. Due to the strong hydration of polyMPDSAH, the adsorption of oil droplets would require water to be removed from the charge units in expanded polyMPDSAH chains and only occur when the electrostatic attraction between oil droplets and –$^{+}N(CH_3)_2$ or –SO_3^- groups was larger than the hydration of polyMPDSAH layer. The values of dehydration energy of the membrane were independent on pH environment, as demonstrated in our preceding study [7]. From Fig. 8(c), the MMCP-40 showed the relatively low flux in the end of each filtration cycle at pH 4 and pH 8. Because the filtration performance of MMCP-40 in the pure water was independent on the pH environment, as shown in Fig. 8(c) (the first point), it could be explained by the fact that the property of oil droplets was frequently similar to that of proteins, having an isoelectric point [28]. Then, the oil droplets (pI 5.7) exhibited net positive and negative charge at pH 4 and pH 8, respectively. Electrostatic interaction between charged oil droplets and –SO_3^- or –$^{+}N(CH_3)_2$ groups in expanded polyMPDSAH chains at pH 4 and pH 8 leaded to the oil droplets adsorbed onto MMCP-40, as a result, the increase in pressure loading during the filtration made

Table 5
Rejection (R_1, %) and relative flux recovery (RFR_1, %) of various membranes after the 1st cycle filtration of the oil-in-water emulsion with different pH and NaCl concentration

	R_1 (%)					RFR_1 (%)				
Code	pH 4 40 mmol/L NaCl	pH 6 40 mmol/L NaCl	pH 8 40 mmol/L NaCl	pH 6 0 mmol/L NaCl	pH 6 20 mmol/L NaCl	pH 4 40 mmol/L NaCl	pH 6 40 mmol/L NaCl	pH 8 40 mmol/L NaCl	pH 6 0 mmol/L NaCl	pH 6 20 mmol/L NaCl
M0	30.0	30.2	29.8	33.1	32.8	53.4	53.2	52.7	53.4	55.4
MMCP	43.5	41.1	43.6	32.5	39.6	85.9	86.0	86.2	56.2	70.9
MMCP-10	52.3	48.7	50.6	42.6	45.7	90.3	91.3	89.3	65.3	79.8
MMCP-20	59.8	57.4	60.5	53.4	56.2	91.4	93.4	92.8	66.8	81.2
MMCP-30	73.3	72.1	73.8	58.7	66.4	88.2	96.9	89.5	79.9	89.5
MMCP-40	83.4	83.6	84.1	63.4	77.8	81.5	98.2	81.1	89.7	95.8
MMCP-50	83.0	83.3	84.3	63.6	77.4	81.6	98.3	82.4	89.4	95.6
MMCP-60	83.5	83.8	83.9	63.5	77.5	82.3	98.3	82.0	89.2	94.9

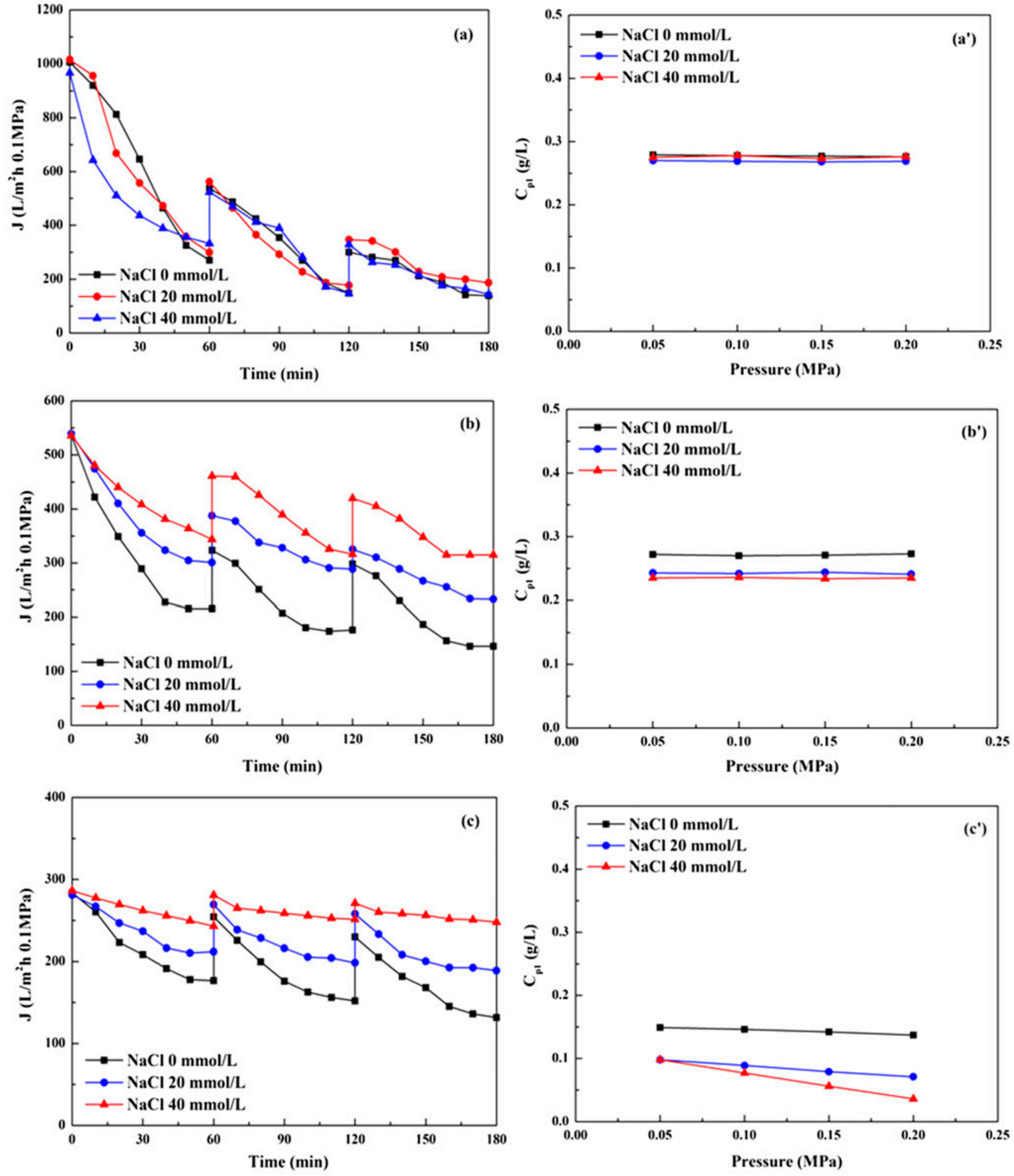

Fig. 9. Filtration decline behavior and permeate concentration after 1st cycle filtration of (a–a´) M0, (b–b´) MMCP, and (c–c´) MMCP-40 in the oil-in-water emulsion with different NaCl concentration (at pH 6).

very few contributions to enhancing the membrane rejection, as shown in Fig. 8(c´). Additionally, the adsorption of oil droplets onto the M0 and MMCP surfaces through the hydrophobic interaction caused the few influences of the pressure loading on the membrane rejection, which can be seen from Fig. 8(a´) and (b´).

According to the data in Table 5, it can be found that the M0 and MMCP showed the poor oil separation with the oil rejection of ≈30 and 42%, respectively at various pH. The complete stretch of polyMPDSAH layers on MMCP-40 resulted in the twice high rejection of >80%. In addition, after the oil solution filtration in each circle, the membranes were washed and then the pure water fluxes were measured again. The values can be used to calculate the relative flux recovery ($\mathrm{RFR}_{i\ (i=1,2)}$). The RFR_i defined as the ratio of pure water flux in the *i*th cycle to that in the initial process can reveal the extent of cleaning efficiency and the effect of irreversible fouling resistance of the membrane [17,23]. The higher value of RFR_i indicated the lower persistent oil adsorption to the membrane operated during the *i*th cycle. The RFR_1 value of M0 was ≈53% due to the membrane fouling caused by the hydrophobicity of PVDF. The grafted polyMPDSAH on the surface and subsurface of membrane contributed to the improvement of irreversible fouling resistance for MMCP, which showed the relatively high RFR_1 value (≈86%). The RFR_1 values of MMCP-10–MMCP-60 were more than 90% at pH 6, indicating that the swelling of polyMPDSAH layers improved the anti-fouling performance of membrane further. Moreover, unlike M0 and MMCP, the RFR_1 values of MMCP-10–MMCP-60 depended on the pH environment greatly. The RFR_1 values at pH 4 and pH 8 were lower than that at pH 6, which was consistent to the results of flux permeate.

For the cyclic filtration of the oily water without NaCl, the flux of MMCP exhibited a similar RFR_1 (56.2%) to M0 (53.4%), which can be seen in Table 5. It indicated that the resistance to the oil fouling was hardly improved by the PSB-grafted PVDF membrane during the filtration of oily water. However, during the filtration of the oily water containing 40 mmol/L of NaCl, the MMCP demonstrated a better flux recovery capability (Fig. 9(b)) and the RFR_1 increased to 86.0%, which can be attributed to the anti-oil-fouling performance of the membrane from the slight swelling of polyMPDSAH in the oil solution. For MMCP-40, the complete swelling of polyMPDSAH on the surface and subsurface of membrane formed a sieving layer not only to reject the oil droplets, but also to resist the membrane fouling. The increase in the NaCl concentration in the oily water showed favor to the complete stretching of polyMPDSAH, which hindered the flux decline and enhanced the R_1 and RFR_1, as shown in Fig. 9(c) and Table 5. Although, the droplet size of oil droplets decreased slightly with the increase in the NaCl concentration in the oily water, as shown in Table 2, which was beneficial to increase the flux recovery of the membrane during the filtration of the oily water containing more NaCl. However, the increase in rejection with the increase in the NaCl concentration in the oily water (Table 5) confirmed the contribution of the swelling of polyMPDSAH to the rejection and anti-fouling performances of the membrane. Moreover, according to the definition of D_v 10 in Table 2, the number of the droplets whose size were more than 1.84 μm accounts for 90 percent of the total in the oily water with 40 mmol/L NaCl and at pH 6. As shown in Table 5, the rejection of 83.6% for the membrane (MMCP-40) indicated that most of oil droplets (more than 90%) were rejected by the membrane while the soluble oil permeated through the membrane. It is expected to reject both oil droplet and soluble oil by adding the flocculant in the oily water system.

In summary, MMCP-40 showed an ideal performance with high flux recovery (>98%) and oil rejection (>90%) of oil droplets after the filtration of the oily water with 40 mmol/L NaCl and at pH 6. The complete stretching of polyMPDSAH layer on the surface and subsurface of membrane leaded to the pH responsiveness and excellent oil separation performance in oily water.

3.3. *Analysis of fouling mechanisms by Hermia's models*

According to Hermia's models, the pore blocking kinetic models were applied to estimate the fouling characteristics of the membrane systems, i.e. the filtration of the oily water with 40 mmol/L NaCl, and at pH 6 through M0, MMCP, and MMCP-40 in this study. Fig. 10 illustrates the fitting of the experimental results to Hermia's models and the calculated model constants and R^2 values are presented in Table 6. The higher absolute value of model constant means greater extent of the flux change with time, which indicates the worse membrane fouling. The higher R^2 value corresponds to a better fit of the model when it is obtained for the same models to compare the different membranes.

The complete blocking mechanism occurred when the size of oil droplets was greater than the membrane pore size, thus, each particle/oil droplet arriving at the membrane surface membrane blocked a pore without any superposition [32,33]. Fig. 10(a) shows the fitting of the experimental data to the complete pore

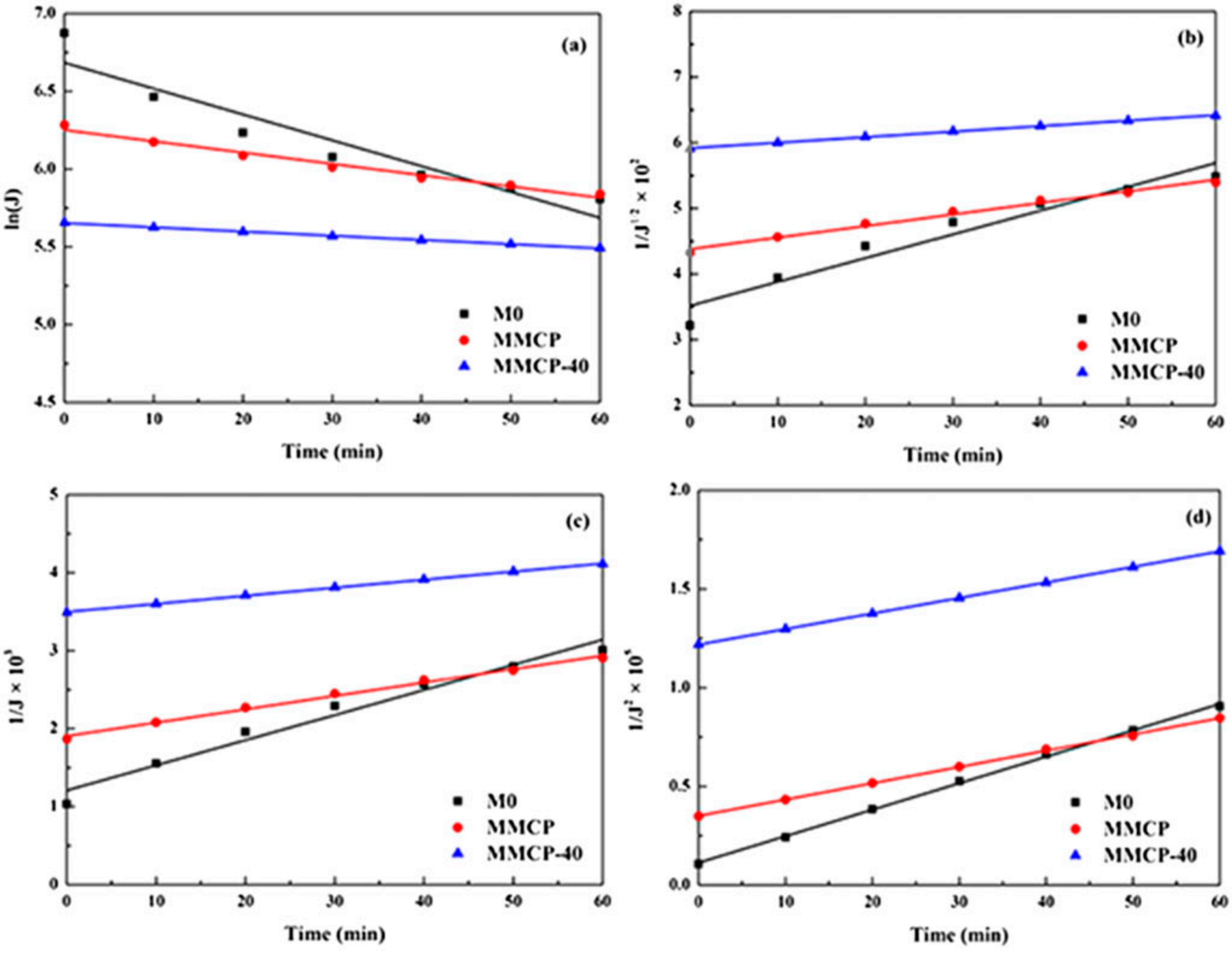

Fig. 10. Permeate flux predicted by the Hermia's models (a) complete pore blocking model, (b) standard pore blocking, (c) intermediate pore blocking, and (d) cake layer formation model (lines: predicted data; symbols: experimental results).

Table 6
Model constants and R^2 values of the Hermia's models for M0, MMCP, MMCP-40

	Complete pore blocking		Standard pore blocking		Intermediate pore blocking		Cake layer formation	
Code	K_{co}	R^2	$K_s \times 10^2$	R^2	$K_i \times 10^3$	R^2	$K_{cl} \times 10^5$	R^2
M0	−0.01661	0.88483	0.03623	0.93285	13.16048	0.96789	0.01341	0.99904
MMCP	−0.00725	0.97742	0.01763	0.98653	7.01919	0.99321	0.00825	0.99922
MMCP-40	−0.00272	0.99763	0.00839	0.99722	4.22213	0.99948	0.00787	0.99996

blocking model for different membranes. For M0, the fitting of the complete pore blocking model to the experimental data was not well acceptable, which could be attributed to the fact that the high pore size (SMp = 0.109 μm) of M0 made many oil droplets permeate through the membrane. For MMCP-40, although the much smaller pore size (SMp = 0.010 μm) contributed to the best agreement of the fitted results with the experimental data, the R^2 value was still less than 0.999.

When the size of oil droplets was smaller than that of the membrane pores, the standard pore blocking often occurred [33]. The adsorption of oil droplets onto the membrane pore walls resulted in the internal pore blocking. Fig. 10(b) indicates that difference between experimental data and the fitted results was still largest for M0 because the oil droplets were retained by the membrane through the hydrophobic interaction, which was revealed by the behavior of permeate flux decline in Fig. 8(a) In addition, the R^2 value of MMCP-40 (Table 6) was still not high enough (<0.999) since the membrane pores were smaller than the oil droplets in the feed solution.

If the membrane pore size was similar to the size of oil droplets, intermediate pore blocking would occur. In such a case, each droplet arriving at the membrane surface might sit on another previously arrived droplet or it might directly block some other portion of the membrane area. As shown in Fig. 10(c) and Table 6, the intermediate pore blocking model provided good agreement with the experimental data for MMCP-40 which had a high R^2 value of >0.999, because the intermediate pore blocking model described more accurately a real UF process than the complete pore blocking model [28,31,34–36]. In the other words, this result further proved the typical UF performance of MMCP-40.

Cake layer formed on the membrane surface when oil droplets were much greater than the membrane pore size. In this situation, all of the membrane pores have been already blocked and oil droplet arriving to the surface of membrane deposited on other droplets, resulting in a cake layer which grew with time and therefore caused further flux decline. Fig. 10(d) shows the fitting of the cake layer formation model to the experimental data according to the corresponding equation in Table 3. The values of R^2 in Table 6 were all >0.999 for M0, MMCP, and MMCP-40. For the three of membrane tested, the model predictions were in good agreement with the experiment data because most of oil droplets were retained over the hydrophobic surface or the hydrophilic sieving layer of the membranes, especially for MMCP-40.

In sum, for M0 and MMCP, high deviations between the experimental and predicted permeation flux can be observed for cake filtration model. The result showed that the cake formation model gave the best agreement with experimental data for MF membranes in this study. The performance data for MMCP-40 indicated that the good prediction of permeation flux was achieved using the intermediate pore blocking and cake formation models. Therefore, it can be concluded that the best fitting to the experimental data corresponded to the cake layer formation

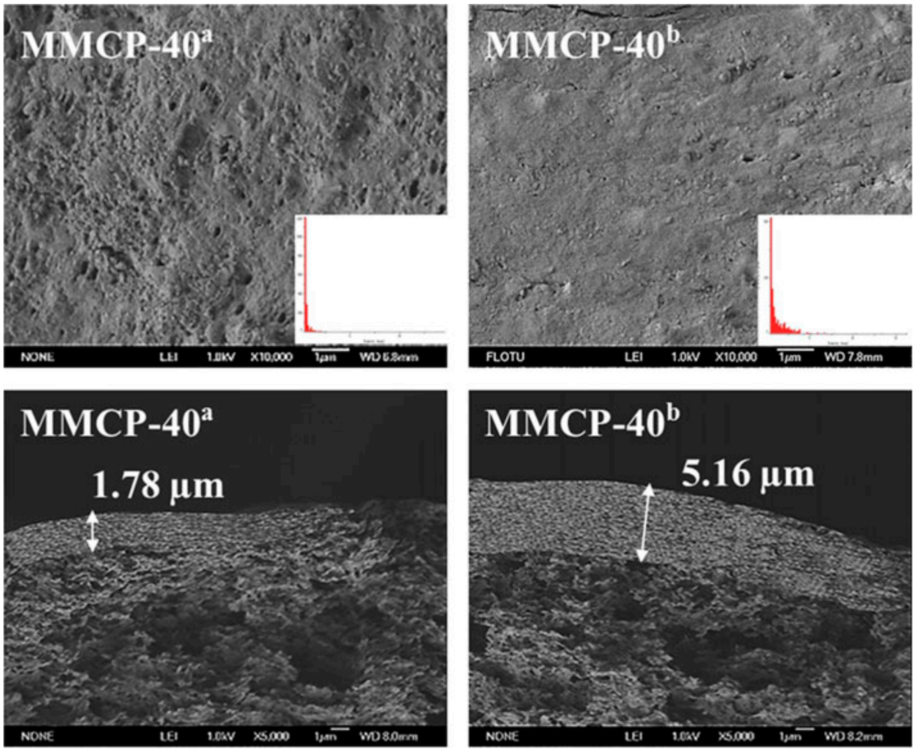

Fig. 11. SEM images of the outside surfaces (upside) and the outer cross sections (downside) of MMCP-40^a, MMCP-40^b.

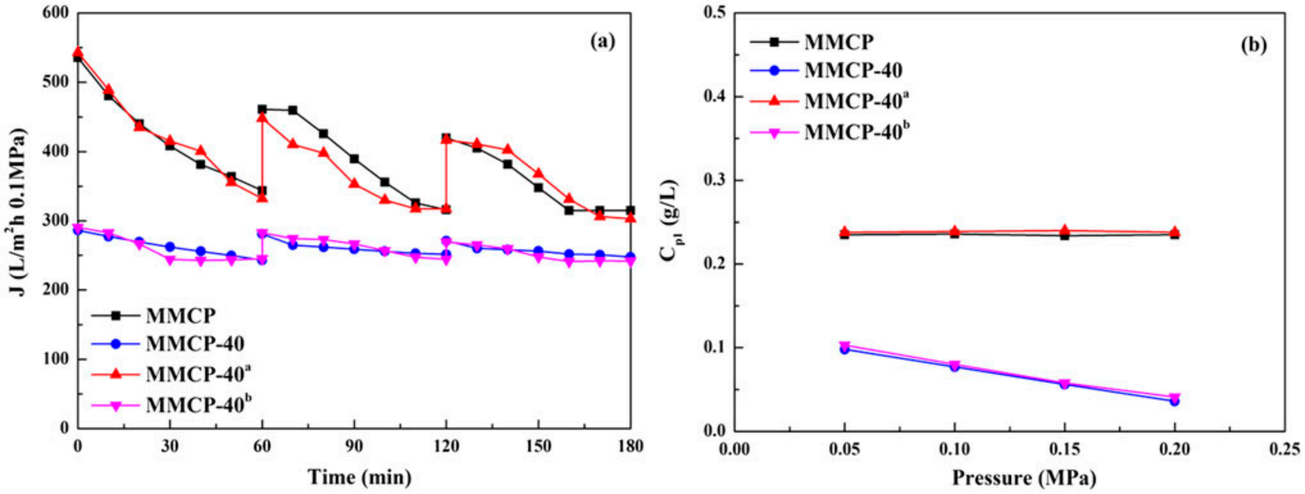

Fig. 12. (a) Filtration decline behavior and (b) permeate concentration after 1st cycle filtration of MMCP, MMCP-40, MMCP-40^a, and MMCP-40^b in the oil-in-water emulsion with 40 mmol/L NaCl and at pH 6.

model for the MF membrane and the UF membrane in this study. It should be noted that although the intermediate pore blocking and cake formation mechanisms were combined to make the oil droplets deposit over the surface of MMCP-40, the hydrophilic sieving layer of polyMPDSAH hindered the permanent adsorption of oil droplets on the membrane surface, resulting in a strong capability of flux recovery as shown in Table 5.

3.4. Smart behavior of the PSB UF membrane on oil removal

To evaluate the smart behavior, the PSB UF membrane MMCP-40 was immersed in pure water at 25˚C for 48 h (MMCP-40^a) and 40 mmol/L NaCl solution at 60˚C for 24 h (MMCP-40^b) alternately. The SEM images of the outside surfaces cross section of MMCP-40^a and MMCP-40^b are shown in Fig. 11. For MMCP-40^a, the Na^+ and Cl^- ions captured by polyMPDSAH were removed and the intra- and/or inter-chain associations reformed. As a result, the polyMPDSAH layer on and in MMCP-40^a displayed a collapsed structure and reduced the thickness (1.78 μm). After immersed in 40 mmol/L NaCl solution at 60˚C for 24 h again, the surface morphology and sieving layer thickness (5.16 μm) of MMCP-20NC-60^b recovered, which can be observed from Fig. 11.

Fig. 12 indicates that the flux of MMCP-40^a increased, which was comparable to that of MMCP. It meant that the surface pores of MMCP-40 ^{a} "opened" to make most of oil droplets pass. For MMCP-40^b, the rejection for oil droplets increased and the degree of flux decline reduced obviously because the polyMPDSAH chains re-stretched as a sieving layer to retain the oil droplets and reduced the membrane fouling. In this case, the surface pores of membrane "closed".

In short, the MMCP and MMCP-40^a can permeate most of oil droplets, while the MMCP-40 and MMCP-40^b can be applied to separate the oily water with excellent separation efficiency and anti-oil-fouling performance. Therefore, a UF membrane with the controllable selectivity for oily wastewater can be obtained by means of the simple immersion/washing method.

4. Conclusions

A PSB hollow fiber UF membrane with a smart "opened"/"closed" structure and controllable selectivity for oily water was obtained by altering the structure of polyMPDSAH layer. The higher NaCl concentration increased the thickness of swelled polyMPDSAH layer on the surface and subsurface of PVDF membrane. The sieving layer of the PSB UF membrane could stretch completely and the thickness of it was more than 5 μm after immersed in 40 mmol/L NaCl solution, which contributed to the greatly improved hydrophilicity, membrane strength, and thermal property. The complete stretching of polyMPDSAH layers on the surface and subsurface of membrane leads to excellent separation performance of the UF membrane in oily water. At pH 6, the PSB UF membrane showed an ideal performance with high flux recovery (>98%) and oil rejection (>80%) after the filtration of the oily water with 40 mmol/L NaCl. The results of oil droplet size indicated that more than 90% of oil droplets were rejected by the membrane while the soluble oil permeates through the membrane. The PSB UF membrane expanded the membrane application in the batch treatment of oily wastewater and purification of water. In the further study, the filtration performance of real oily wastewater through such UF membrane should be investigated systematically because the trade-off between hydration and resistance vs. dehydration and interaction of polyMPDSAH chains in the real oily wastewater will become much more complex.

Acknowledgments

This work was supported by National Key Technologies R&D Program of China (2015BAE06B00) and Tsinghua University Initiative Scientific Research Program (20121088039).

Abbreviations

A — outside surface area of the membrane
ATR — attenuated total reflectance
$C_{f(p)_i}$ — protein concentrations in the feed (*f*) and permeate (*p*) solutions after *i*th cycle filtration
d — apparent pore diameter of membrane
$D_{\text{cut-off}}$ — pore diameter from MWCO calculated by hydrodynamic diameter of dextran or PEO
DSC — differential scanning calorimetry
FTIR — Fourier transform infrared
FWF — free water fraction
HCl — hydrochloric acid
i — *i*th filtration
$J_{v,i}$, — permeate flux of oily water during *i*th filtration
$J_{v_{H_2O},i}$ — permeate flux of pure water during *i*th filtration
K_{Cl} — cake layer formation model constant
K_{co} — complete pore blocking model constant
K_i — intermediate pore blocking model contant
K_s — standard pore blocking model contant
M0 — nascent PVDF membrane
MCP — PVDF-cl-PVP membrane
MF — microfiltration
MMCP — polyMPDSAH-g-PVDF-cl-PVP membrane
MMCP-10 — MMCP membrane after swelling in the 10 mmol/L NaCl solution
MMCP-20 — MMCP membrane after swelling in the 20 mmol/L NaCl solution
MMCP-30 — MMCP membrane after swelling in the 30 mmol/L NaCl solution
MMCP-40 — MMCP membrane after swelling in the 40 mmol/L NaCl solution
MMCP-50 — MMCP membrane after swelling in the 50 mmol/L NaCl solution
MMCP-60 — MMCP membrane after swelling in the 60 mmol/L NaCl solution
MPDSAH — 3-(methacryloylamino) propyl-dimethyl-(3-sulfopropyl) ammonium hydroxide
M_W — molecular weight
MWCO — molecular weight cut-off
NaCl — sodium chloride
NaOH — sodium hydroxide
PEO — polyethylene oxide
pI — isoelectric point
polyMPDSAH — poly(3-(methacryloylamino) propyl-dimethyl-(3-sulfopropyl) ammonium hydroxide)
PSB — sulfobetaine polymer
PVDF — poly(vinylidene fluoride)
PVP — poly(vinyl pyrrolidone)
RFR_i — relative flux recovery during *i*th filtration
R_i — rejection during *i*th filtration
RMS — mean surface roughness
SB — sulfobetaine
SEM — scanning electron microscope
SMP — surface mean pore size
TOC — total organic carbon
UF — ultrafiltration
XPS — X-ray photoelectron spectroscopy
ZnSe — zinc selenide
Δt — permeation time
ρ — solution density

References

[1] H.X. Zhao, H.F. Li, H.T. Yu, H.M. Chang, X. Quan, S. Chen, CNTs-TiO_2/Al_2O_3 composite membrane with a photocatalytic function: Fabrication and energetic performance in water treatment, Sep. Purif. Technol. 116 (2013) 360–365.

[2] Y.Q. Pan, T.T. Wang, H.M. Sun, W. Wang, Preparation and application of titanium dioxide dynamic membranes in microfiltration of oil-in-water emulsions, Sep. Purif. Technol. 89 (2012) 78–83.

[3] E. Yuliwati, A.F. Ismail, Effect of additives concentration on the surface properties and performance of PVDF ultrafiltration membranes for refinery produced wastewater treatment, Desalination 273 (2011) 226–234.

[4] A. Asatekin, A.M. Mayes, Oil industry wastewater treatment with fouling resistant membranes containing amphiphilic comb copolymers, Environ. Sci. Technol. 43 (2009) 4487–4492.

[5] Y.Q. Zhang, P. Cui, T.D. Du, L.B. Shan, Y.L. Wang, Development of a sulfated Y-doped nonstoichiometric zirconia/polysulfone composite membrane for

treatment of wastewater containing oil, Sep. Purif. Technol. 70 (2009) 153–159.

[6] S.M. Santos, M.R. Wiesner, Ultrafiltration of water generated in oil and gas production, Water Environ. Res. 69 (1997) 1120–1127.

[7] Q. Li, Q.Y. Bi, H.H. Lin, L.X. Bian, X.L. Wang, A novel ultrafiltration (UF) membrane with controllable selectivity for protein separation, J. Membr. Sci. 427 (2013) 155–167.

[8] J. Yang, D.W. Li, Y.K. Lin, X.L. Wang, F. Tian, Z. Wang, Formation of a bicontinuous structure membrane of polyvinylidene fluoride in diphenyl ketone diluent via thermally induced phase separation, J. Appl. Polym. Sci. 110 (2008) 341–347.

[9] Q. Li, Z.L. Xu, L.Y. Yu, Effects of mixed solvents and PVDF types on performances of PVDF microporous membranes, J. Appl. Polym. Sci. 115 (2010) 2277–2287.

[10] M. Zhang, L. Zhang, L.H. Cheng, K. Xu, Q.P. Xu, H.L. Chen, J.Y. Lai, K.L. Tung, Extracorporeal endotoxin removal by novel l-serine grafted PVDF membrane modules, J. Membr. Sci. 405–406 (2012) 104–112.

[11] Y.H. Zhao, K.H. Wee, R.B. Bai, A novel electrolyte-responsive membrane with tunable permeation selectivity for protein purification, ACS Appl. Mater. Interfaces 2 (2010) 203–211.

[12] Y.F. Yang, Y. Li, Q.L. Li, L.S. Wan, Z.K. Xu, Surface hydrophilization of microporous polypropylene membrane by grafting zwitterionic polymer for anti-biofouling, J. Membr. Sci. 362 (2010) 255–264.

[13] G.Q. Zhai, S.C. Toh, W.L. Tan, E.T. Kang, K.G. Neoh, C.C. Huang, D.J. Liaw, Poly(vinylidene fluoride) with grafted zwitterionic polymer side chains for electrolyte-responsive microfiltration membranes, Langmuir 19 (2003) 7030–7037.

[14] Y.L. Su, L.L. Zheng, C. Li, Z.Y. Jiang, Smart zwitterionic membranes with on/off behavior for protein transport, J. Phys. Chem. B 112 (2008) 11923–11928.

[15] Y. Chang, S. Chen, Z. Zhang, S. Jiang, Highly protein-resistant coatings from well-defined diblock copolymers containing sulfobetaines, Langmuir 22 (2006) 2222–2226.

[16] Q. Li, Q.Y. Bi, T.Y. Liu, X.L. Wang, Resistance to protein and oil fouling of sulfobetaine-grafted poly(vinylidene fluoride) hollow fiber membrane and the electrolyte-responsive behavior in NaCl solution, Appl. Surf. Sci. 258 (2012) 7480–7489.

[17] M.Z. Li, J.H. Li, X.S. Shao, J. Miao, J.B. Wang, Q.Q. Zhang, X.P. Xu, Grafting zwitterionic brush on the surface of PVDF membrane using physisorbed free radical grafting technique, J. Membr. Sci. 405–406 (2012) 141–148.

[18] Y.C. Chiang, Y. Chang, A. Higuchi, W.Y. Chen, R.C. Ruaan, Sulfobetaine-grafted poly(vinylidene fluoride) ultrafiltration membranes exhibit excellent antifouling property, J. Membr. Sci. 339 (2009) 151–159.

[19] Y. Chang, W.J. Chang, Y.J. Shih, T.C. Wei, G.H. Hsiue, Zwitterionic sulfobetaine-grafted poly(vinylidene fluoride) membrane with highly effective blood compatibility via atmospheric plasma-induced surface copolymerization, ACS Appl. Mater. Interfaces 3 (2011) 1228–1237.

[20] Z. Zhang, S. Chen, Y. Chang, S. Jiang, Surface grafted sulfobetaine polymers via atom transfer radical polymerization as superlow fouling coatings, J. Phys. Chem. B 110 (2006) 10799–10804.

[21] J. Zhao, Q. Shi, S.F. Luan, L.J. Song, H.W. Yang, H.C. Shi, J. Jin, X.L. Li, J.H. Yin, P. Stagnaro, Improved biocompatibility and antifouling property of polypropylene non-woven fabric membrane by surface grafting zwitterionic polymer, J. Membr. Sci. 369 (2011) 5–12.

[22] Q.F. Zhang, S.B. Zhang, L. Dai, X.S. Chen, Novel zwitterionic poly(arylene ether sulfone)s as antifouling membrane material, J. Membr. Sci. 349 (2010) 217–224.

[23] L.J. Wang, Y.L. Su, L.L. Zheng, W.J. Chen, Z.Y. Jiang, Highly efficient antifouling ultrafiltration membranes incorporating zwitterionic poly ([3-(methacryloylamino) propyl]-dimethyl (3-sulfopropyl) ammonium hydroxide), J. Membr. Sci. 340 (2009) 164–170.

[24] H.J. Yu, Y.M. Cao, G.D. Kang, J.H. Liu, M. Li, Q. Yuan, Enhancing antifouling property of polysulfone ultrafiltration membrane by grafting zwitterionic copolymer via UV-initiated polymerization, J. Membr. Sci. 342 (2009) 6–13.

[25] Q. Li, Q.Y. Bi, B. Zhou, X.L. Wang, Zwitterionic sulfobetaine-grafted poly(vinylidene fluoride) membrane surface with stably anti-protein-fouling performance via a two-step surface polymerization, Appl. Surf. Sci. 258 (2012) 4707–4717.

[26] O. Azzaroni, A.A. Brown, W.T.S. Huck, UCST wetting transitions of polyzwitterionic brushes driven by self-association, Angew. Chem. Int. Ed. 45 (2006) 1770–1774.

[27] P. Mary, D.D. Bendejacq, M.P. Labeau, P. Dupuis, Reconciling low- and high-salt solution behavior of sulfobetaine polyzwitterions, J. Phys. Chem. B 111 (2007) 7767–7777.

[28] R.E. Holmlin, X.X. Chen, R.G. Chapman, S.C. Takayama, G.M. Whitesides, Zwitterionic SAMs that resist nonspecific adsorption of protein from aqueous buffer, Langmuir 17 (2001) 2841–2850.

[29] P.D. Peeva, N. Million, M. Ulbricht, Factors affecting the sieving behavior of anti-fouling thin-layer cross-linked hydrogel polyethersulfone composite ultrafiltration membranes, J. Membr. Sci. 390–391 (2012) 99–112.

[30] M.N. Sarbolouki, A general diagram for estimating pore size of ultrafiltration and reverse osmosis membranes, Sep. Sci. Technol. 17 (1982) 381–386.

[31] Q. Li, B. Zhou, Q.Y. Bi, X.L. Wang, Surface modification of PVDF membranes with sulfobetaine polymers for a stably anti-protein-fouling performance, J. Appl. Polym. Sci. 125 (2012) 4015–4027.

[32] A. Salahi, A. Gheshlaghi, T. Mohammadi, S.S. Madaeni, Experimental performance evaluation of polymeric membranes for treatment of an industrial oily wastewater, Desalination 262 (2010) 235–242.

[33] A. Salahi, M. Abbasi, T. Mohammadi, Permeate flux decline during UF of oily wastewater: Experimental and modeling, Desalination 251 (2010) 153–160.

[34] A. Salahi, R. Badrnezhad, M. Abbasi, T. Mohammadi, F. Rekabdar, Oily wastewater treatment using a hybrid UF/RO system, Desalin. Water Treat. 28 (2011) 75–82.

[35] L.E. Fratila-Apachitei, M.D. Kennedy, J.D. Linton, I. Blume, J.C. Schippers, Influence of membrane morphology on the flux decline during dead-end ultrafiltration of refinery and petrochemical waste water, J. Membr. Sci. 182 (2001) 151–159.

[36] A. Salahi, T. Mohammadi, Experimental investigation of oily wastewater treatment using combined membrane systems, Water Sci. Technol. 62 (2010) 245–255.